ACS APPLIED MATERIALS & INTERFACES

Research Article

www.acsami.org

Ultrasensitive ROS-Responsive Coassemblies of Tellurium-Containing Molecules and Phospholipids

Lu Wang,[†] Fuqiang Fan,[†,‡] Wei Cao,[†] and Huaping Xu*[,†]

[†]Key Laboratory of Organic Optoelectronics and Molecular Engineering, Department of Chemistry, Tsinghua University, Beijing 100084, People's Republic of China

[‡]The Research Centre for Molecular Science and Engineering, Northeastern University, Shenyang, 110004, People's Republic of China

Supporting Information

ABSTRACT: Reactive oxygen species (ROS) play crucial roles in cell signaling and redox homeostasis and are strongly related to metabolic activities. The increase of the ROS concentration in organisms can result in several diseases, such as cardiovascular diseases and cancer. The concentration of ROS in biologically relevant conditions is typically as low as around tens of micromolars to 100 μM H_2O_2, which makes it necessary to develop ultrasensitive ROS-responsive systems. A general approach is reported here to fabricate an ultrasensitive ROS-responsive system via coassembly between tellurium-containing molecules and phospholipids, combining the ROS-responsiveness of tellurium and the biocompatibility of phospholipids. By using dynamic light scattering, transmission electron microscopy, scanning electron microscopy, and NMR spectra, coassembly behaviors and the responsiveness of the coassemblies have been investigated. These coassemblies can respond to 100 μM H_2O_2, which is a biologically relevant ROS concentration, and demonstrate reversible redox properties.

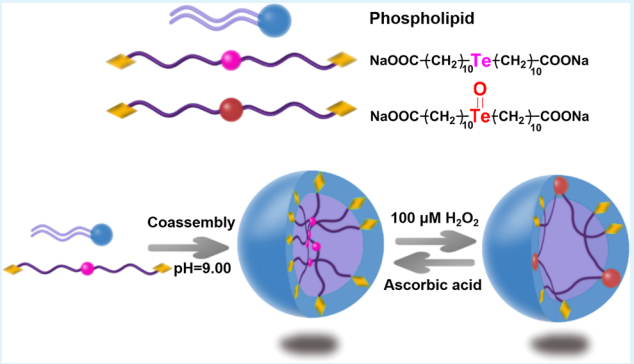

KEYWORDS: *reactive oxygen species, ultrasensitive, phospholipid, tellurium, coassembly*

INTRODUCTION

Reactive oxygen species (ROS), which indicate chemically reactive oxygen-containing ions and free radicals with valence electrons or unstable bonds, are short-lived and tend to react with other molecules.[1−4] ROS are formed as a natural byproduct from cell metabolism, especially from mitochondrial metabolism, and play crucial roles in cell signaling and redox homeostasis.[5−8] Abnormal ROS concentration, either too low or too high, will give rise to diseases.[9,10] The ROS concentration usually rises with the general aging process of cells and results in significant cell damage.[11−13] This is known as oxidative stress, which is considered to be one of the major characteristics of many diseases, including Parkinson's diseases,[14] Alzheimer's disease,[15] cardiovascular diseases,[16] and cancer.[17,18] Besides these diseases, oxidative stress is also related to cell apoptosis, and there have been many studies concentrated on inducing apoptosis in cancer cells as a cancer therapy method.[19−21]

Recently, there have been many drug-delivery-related researches based on targeting ROS generation systems for effective therapy. The NOX family of NADPH oxidases, which can transfer electrons to get through the cell membrane and generate superoxide ions, play important roles in ROS generation.[22] Studies on the inhibition of the NOX family have drawn great attention; however, many inhibitors still need to be improved for better specificity. It is still a challenge to find solutions to control the concentration of ROS.[23] Except for seeking proper inhibitors, another facile way to eliminate ROS is to use ROS-sensitive compounds.[24] Previous work from our group based on ROS-responsive selenium-containing systems has provided some successful examples, including hydrogel[25] and aggregates in the solution phase[26−32] and on the surface.[33]

As another element of chalcogen, tellurium is similar to selenium and has biological activity as tellurocysteine and telluromethionine in fungi.[34] Organotellurium compounds, which are similar to organoselenium compounds, have been employed as glutathione peroxidase mimics[35−37] and described to be promising biomaterials as pharmacological agents for antioxidant and anticarcinogen therapeutics.[38,39] There have been some studies on organotellurium compounds in our group, including coordination-responsive telluride-containing polymers[40] and layer-by-layer films,[41] which can both release cisplatinum in the presence of multiamine-containing molecules (e.g., spermine). It is known that the concentration of ROS present in biologically relevant conditions is typically as low as around tens of micromolars to 100 μM H_2O_2;[42,43] thus, it is

Received: May 21, 2015
Accepted: July 8, 2015
Published: July 8, 2015

DOI: 10.1021/acsami.5b04419
ACS Appl. Mater. Interfaces 2015, 7, 16054−16060

Scheme 1. Ultrasensitive ROS-Responsive Coassemblies of Tellurium-Containing Molecules and Phospholipids

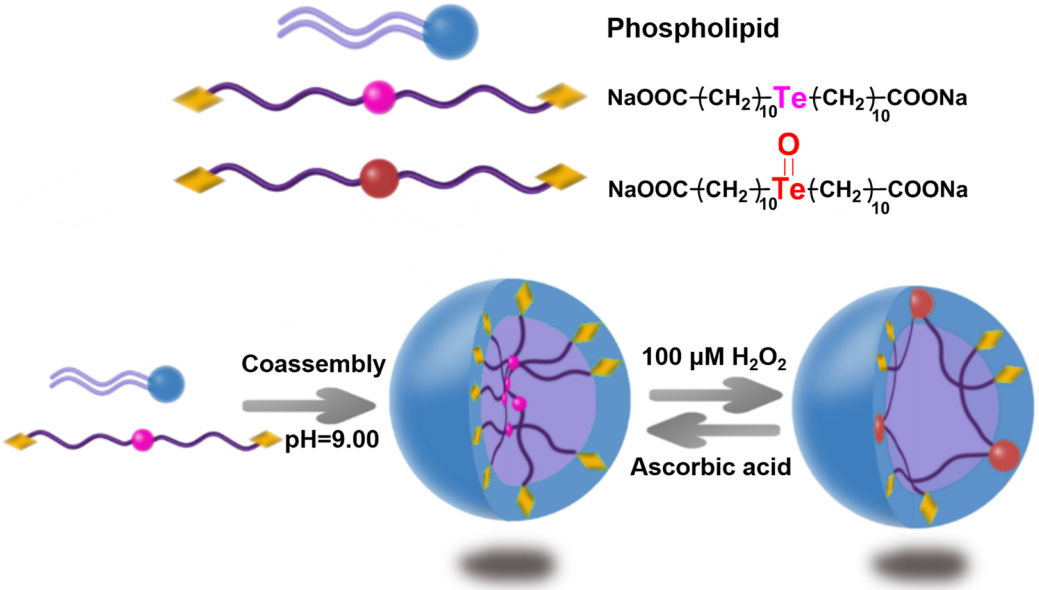

significant to develop oxidation-sensitive materials that show ultrasensitivity to accurately respond to ROS-sufficient positions of the human body.[44] Owing to the ultrasensitive responsiveness to ROS of tellurium-containing polymers,[45] tellurium-containing compounds may be utilized as promising innovative ROS-eliminating materials under physiological environments.

Phospholipid is the main component of the plasma membrane, which plays eminent roles in cellular metabolic activities.[46] It has excellent biocompatibility and biodegradability; therefore, liposome and lipid nanoparticles have been widely used in the drug-delivery area.[47−49] Coassembly, which has been employed to fabricate different kinds of nanostructures (such as nanoparticles, nanofibers, hydrogels, and films) or special materials showing photoelectronic properties or biomedical applications,[32,50−56] is able to integrate both merits of the building blocks and obtain aggregates different from those of either of the individual self-assemblies. We successfully generated ultrasensitive ROS-responsive coassemblies by adding a small portion of tellurium-containing molecules into phospholipids to coassemble. Owing to the reversible redox property of tellurium-containing molecules, the structures of coassemblies expressed a reversible change under redox conditions (as shown in Scheme 1).

EXPERIMENTAL SECTION

Materials. Tellurium powder and sodium borohydride were purchased from Aladdin Chemical Company. 1,2-Diphytanoyl-*sn*-glycero-3-phosphocholine (25 mg/mL, chloroform solution, denoted as DPPC, as shown in Scheme 2a) was purchased from Avanti Polar Lipids. 1,2-Dipalmitoyl-*sn*-glycero-3-phosphoethanolamine (denoted as DPPE, as shown in Scheme 2b) and 11-bromoundecanoic acid were products of TCI. A buffer solution of pH = 9.00 (20 °C, boric acid/potassium chloride/sodium hydroxide) was a product of J&K Scientific Ltd. L-(+)-Ascorbic acid was purchased from Alfa Aesar. Hydrogen peroxide (H_2O_2), other organic solvents, and chemicals used in this work were analytical grade products from Beijing Chemical Reagent Company.

Instrument. The ^1H and ^{13}C NMR spectra were recorded on a JEOL JNM-ECA 400 (400M) spectrometer at 298 and 353 K, respectively. Electrospray ionization mass spectrometry (ESI-MS) spectra were measured on a LTQ LC/MS apparatus.

Scheme 2. Structures of DPPC and DPPE

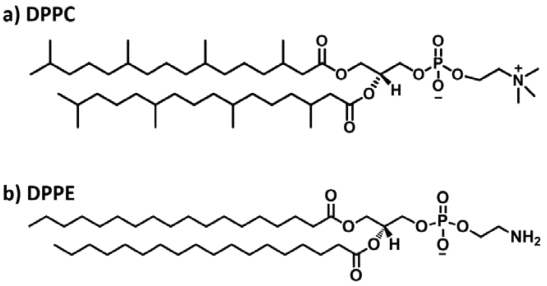

Fluorescence was measured by a Hitachi F-7000 spectrofluorometer.

Dynamic light scattering (DLS) tests were performed at 25 °C on a Malvern 3000HS Zetasizer using a monochromatic coherent He−Ne laser (633 nm) as the light source.

Transmission electron microscopy (TEM) images of the morphology of the aggregates were obtained using a JEM-2010 microscope with an accelerating voltage of 80 kV. Samples were prepared by dropping the aqueous solution on a carbon-coated copper grid for 15 min, followed by staining using 1.5% uranyl acetate. Energy-dispersive spectrometry (EDS) results were obtained by a JEM2010 transmission electron microscope.

Scanning electron microscopy (SEM) images were obtained by a JEOL JSM-7401F field-emission scanning electron microscope operated at 3.0 kV. Samples were prepared by dropping the aqueous solution on the silicon substrate for 15 min.

Synthesis of 11,11′-Tellurodiundecanoic Acid. The tellurium-containing molecule was synthesized via the reaction of disodium telluride and 11-bromoundecanoic acid (Figure S1 in the Supporting Information, SI). Disodium telluride was acquired through the reaction of tellurium powder (2 mmol, 0.255 g) and an excess amount of sodium borohydride (4.4 mmol, 0.166 g) at 41 °C in pure water under an atmosphere of N_2. 11,11′-Tellurodiundecanoic acid (denoted as MTeC10COOH) was prepared by the reaction of disodium telluride and 11-bromoundecanoic acid (4 mmol, 1.06 g) at 41 °C in tetrahydrofuran (THF) under an atmosphere of N_2. After the reaction, THF was evaporated under reduced pressure. Then the product was acidified by HCl, followed by filtration. The filtration residue was washed by dichloromethane to remove soluble impurities. Then the

DOI: 10.1021/acsami.5b04419
ACS Appl. Mater. Interfaces 2015, 7, 16054−16060

residue was redissolved by a mixed solvent of dichloromethane and methanol (CH_3OH; 1:1, v/v), and the filtrate was evaporated by using rotary evaporators. The obtained product was a buff powder (yield 53%).

^{1}H NMR (Figure S2a in the SI; 400 MHz, CD_3OD, 298 K): δ 2.64 (4H, t, TeCH_2), 2.16 (4H, t, CH_2COOH), 1.74 (4H, m, TeCH_2CH_2), 1.60 (4H, m, CH_2CH_2COOH), 1.43−1.29 (24H, m, HOOC$CH_2CH_2(CH_2)_6CH_2CH_2$Te). ^{13}C NMR (Figure S2b in the SI; 400 MHz, DMSO-*d*, 353 K): δ 173.9 (1C, s, COOH), 33.5 (1C, s, CH_2COOH), 31.4 (TeCH_2CH_2), 30.9 (Te$CH_2CH_2CH_2$), 29.0−28.0 (1C, s, Te$CH_2CH_2CH_2(CH_2)_5CH_2CH_2$COOH), 24.2 (1C, s, CH_2CH_2COOH), 1.8 (1C, s, TeCH_2). ESI-MS (Figure S3 in the SI): m/z 499.2 ($[M - H]^-$).

Oxidation and Reduction Experiment of MTeC10COOH. A total of 12.0 mg (0.024 mmol) MTeC10COOH was dissolved in 5 mL CH_3OH, and 5.5 μL of 30% H_2O_2 (0.048 mmol) was added to the solution. Then the flask was sealed by a rubber plug, and the oxidation reaction was carried out at room temperature for 4 h with stirring. CH_3OH was evaporated under reduced pressure. After a ^{1}H NMR test, the oxidized product was redissolved in 10 mL CH_3OH, and 8.46 mg (0.048 mmol) of ascorbic acid was added to the solution. The reduction reaction was carried out at room temperature for another 4 h, and CH_3OH was evaporated under reduced pressure.

Preparation of Different Mass Ratios of Coassemblies. Before fabrication of coassemblies with different mass ratios, 25.0 mg/mL DPPC (chloroform solution) and 5.0 mg/mL MTeC10COOH (methanol solution) were prepared. To fabricate 10:1 DPPC/MTeC10COOH coassemblies, 80 μL of the DPPC solution (2.0 mg of DPPC) and 40 μL of the MTeC10COOH solution (0.2 mg of MTeC10COOH) were mixed under sonication. The solvent was evaporated by a dry nitrogen stream and thoroughly dried in a vacuum oven for another 3 h. Then 4.0 mL of degassed pH = 9.00 aqueous buffer was added, and the hydration process continued overnight at room temperature. The fabrication of other coassemblies was similar; the solutions used were shown in Table 1.

Table 1. Preperation of Different Mass Ratios of Coassemblies

mass ratios of coassemblies	volume (μL) of 25.0 mg/mL DPPC	volume (μL) of 5.0 mg/mL MTeC10COOH	volume (mL) of pH = 9.00 buffer
10:1	80 (2.0 mg)	40 (0.20 mg)	4.0
6:1	80 (2.0 mg)	66 (0.33 mg)	4.0
4:1	80 (2.0 mg)	100 (0.50 mg)	4.0
1:1	80 (2.0 mg)	400 (2.0 mg)	4.0

RESULTS AND DISCUSSION

Oxidation and Reduction Process of MTeC10COOH. The oxidation and reduction process of MTeC10COOH was studied by ^{1}H NMR in CD_3OD, as shown in Figure 1. The chemical shift of α protons of tellurium atoms before oxidation was 2.63 ppm. After oxidation by 2 equiv of H_2O_2, the 2.63 ppm peak disappeared and downshifted to 2.83 ppm. In the presence of 2 equiv of ascorbic acid (Vc), the peak at 2.63 ppm turned up again, which indicated that the tellurium atoms turned to reduced states again. After the oxidation and reduction process, the peak for α protons of the carboxylic groups shifted from 2.14 to 2.16 ppm, which may be attributed to ascorbic acid (Vc) which can influence the pH of the system and further influence the amount of negative charge on the

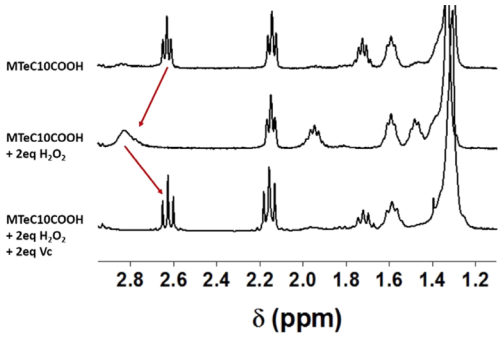

Figure 1. ^{1}H NMR spectra (CD_3OD, 400 M, 298 K) for the redox process of MTeC10COOH.

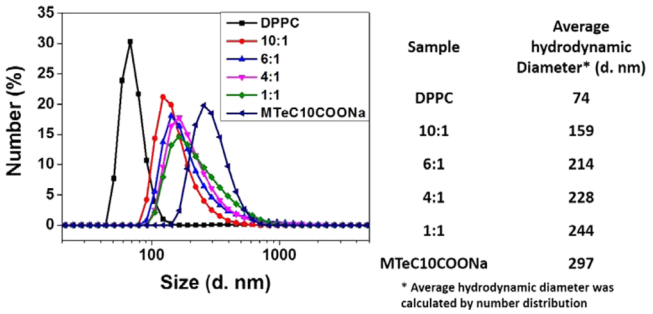

Figure 2. Size distribution and average hydrodynamic diameters of coassemblies with different mass ratios.

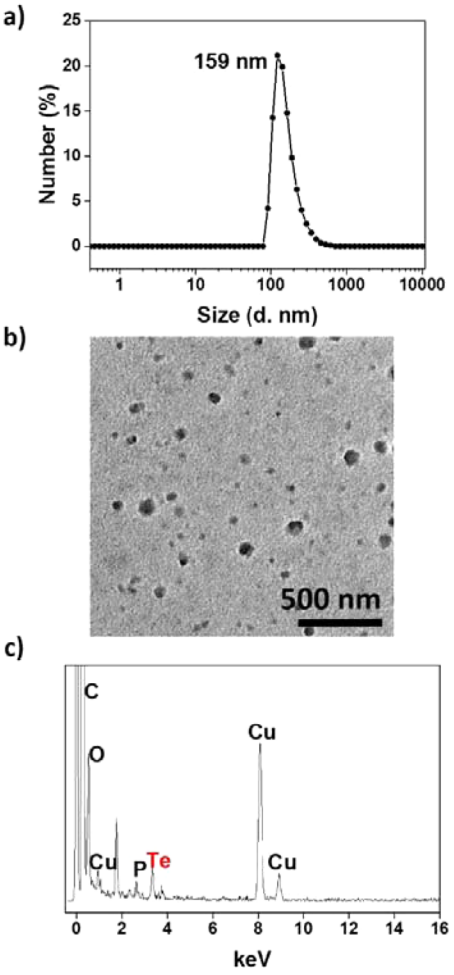

Figure 3. Coassembly behaviors of 10:1 coassemblies: (a) results of DLS measurement; (b) TEM image stained by uranyl acetate; (c) EDS measurement to determine the content of tellurium.

DOI: 10.1021/acsami.5b04419
ACS Appl. Mater. Interfaces 2015, 7, 16054−16060

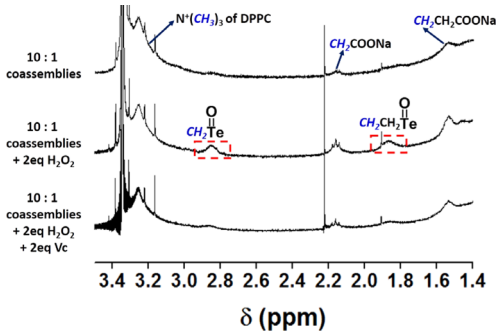

Figure 4. ^{1}H NMR (D_2O, 400 M, 298 K) for redox process of 10:1 coassemblies.

carboxylic groups. The oxidation and reduction process showed that MTeC10COOH can be reversibly oxidized and reduced.

Self-Assembly Properties of DPPC and MTeC10COONa. In an alkali aqueous solution (pH = 9.00 buffer), DPPC and MTeC10COONa can self-assemble on account of their amphiphilic nature, respectively. The critical micelle concentration (CMC) of DPPC was measured by fluorescence using pyrene as the probe. The results showed that the CMC of DPPC was 3×10^{-3} mM. Via DLS, the average hydrodynamic diameter of the assemblies was found to be approximately 74 nm (Figure S4a in the SI). Also the average diameter in the TEM image was 45 nm (Figure S4b in the SI). The results indicated that the assemblies were spherical micelles. Similarly, the CMC of MTeC10COONa was determined to be 4×10^{-1} mM. The average hydrodynamic diameter measured by DLS was 297 nm, as shown in Figure S5a in the SI. The TEM image is shown in Figure S5b in the SI, and the average diameter was 64 nm, which was consistent with the results of DLS for MTeC10COONa self-assembled in spherical micelles.

Coassembly Behaviors of DPPC and MTeC10COONa. It is known that phospholipids tend to form vesicles. Because adding detergent into phospholipid aggregates may cause a phase transition such as that from vesicle to micelle,[57−61] we try to use MTeC10COONa, which is an amphiphilic detergent, to obtain coassemblies with phospholipids and adjust the structures of the coassemblies.

Owing to the hydrophobic and electrostatic interactions between DPPC and MTeC10COONa, they can successfully coassemble in an alkali aqueous solution. Size distributions of coassemblies with different mass ratios were measured by DLS. As shown in Figure 2, all of the average hydrodynamic diameters were between self-assemblies of DPPC and MTeC10COONa. As more and more MTeC10COONa was added to the system, the average hydrodynamic diameters of the coassemblies showed an increasing trend. Dispersion of the size distributions increased at the same time. The phenomenon indicated that the size distributions and average hydrodynamic diameters of coassemblies were positively correlated with the relative content of MTeC10COONa of the system, which showed the generation of new aggregates in the system and can indirectly prove the coassembly process.

The coassembly behaviors of coassemblies with different mass ratios were studied in detail, and the results are shown in Figure 3 (DPPC and MTeC10COONa as a mass ratio of 10:1 and a molar ratio of 6:1) and S7 in the SI (mass ratios of 4:1 and 1:1). Employing a 10:1 coassembly as an example, via DLS, the average hydrodynamic diameter of the aggregates was determined to be 159 nm (Figure 3a), which was between that of DPPC and MTeC10COONa themselves. The TEM results

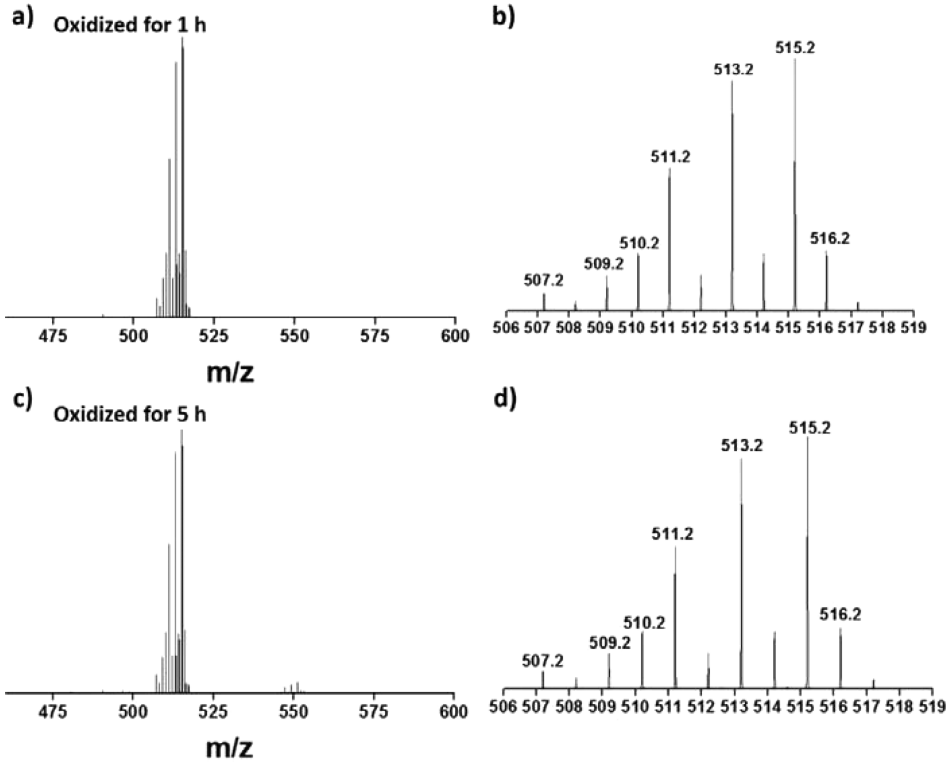

Figure 5. ESI-MS spectra (negative spectra) for 10:1 coassemblies oxidized by 100 μM H_2O_2: (a) oxidized for 1 h; (b) amplified scheme of part a; (c) oxidized for 5 h; (d) amplified scheme of part c.

DOI: 10.1021/acsami.5b04419
ACS Appl. Mater. Interfaces 2015, 7, 16054−16060

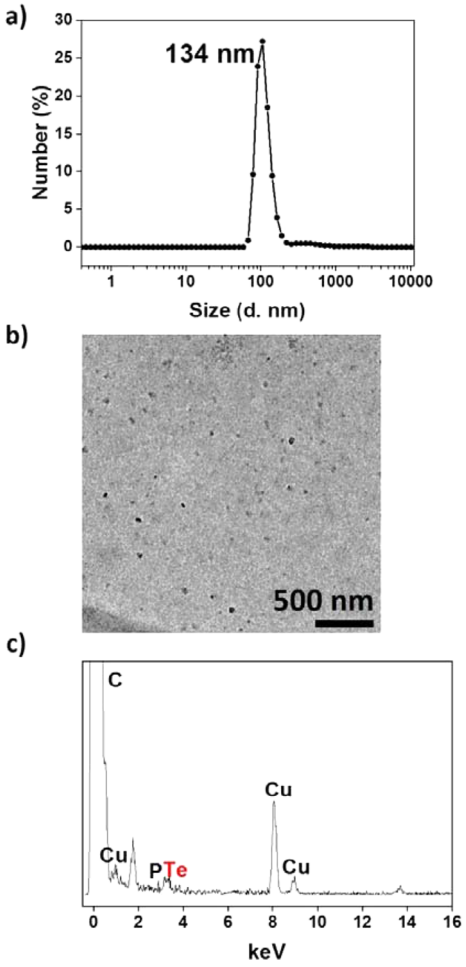

Figure 6. Coassembly behaviors of 10:1 coassemblies between DPPE and MTeC10COONa: (a) results of DLS measurement; (b) TEM image stained by uranyl acetate; (c) EDS measurement to determine the content of tellurium.

are shown in Figure 3b, and the average diameter was around 57 nm. Owing to the aqueous environment of the coassemblies, the average hydrodynamic diameter characterized by DLS was affected by the hydration effect of water. Thus, the results of TEM (Figure 3b) and SEM (Figure S6 in the SI) images seemed smaller than that of DLS. To further prove the coassembly behaviors, EDS was employed to detect the content of tellurium (Figure 3c). The results indicated that there was tellurium in the coassemblies, which can also prove the successful coassembly.

Reversible Oxidation and Reduction of Coassemblies. Owing to the reversible redox nature of MTeC10COONa, it was of significance to investigate the redox properties of the coassemblies. To achieve the ^{1}H NMR experiment, the hydration process of the coassembly was conducted in a D_2O buffer, and the content of the molecules was much concentrated to achieve a better signal in ^{1}H NMR measurement. For example, in 10:1 coasssemblies, the concentrations of DPPC and MTeC10COONa were 5.0 and 0.50 mg/mL, respectively. After removal of the solvent, 3.0 mL of a D_2O buffer was added, and the system was stirred overnight at room temperature. As shown in Figure 4, peaks at 2.16 and 1.53 ppm were for α and β protons of the carboxylic group, respectively. There was no peak for α nor β protons of tellurium atoms of the original 10:1 coassemblies. After the addition of 2 equiv of H_2O_2, new peaks at 2.85 and 1.87 ppm appeared, which each represented the α and β protons of tellurium atoms of the oxidized states. Upon reduction by 2 equiv of Vc, the new peaks disappeared again. To explain the phenomenon, we put forward an assumption. Before oxidation, MTeC10COONa molecules may be encapsulated in the coassemblies, which resulted in the disappearance of the α and β protons of tellurium atom signals. After oxidation by H_2O_2, the tellurium atoms changed to the oxidized states, with increased hydrophilicity, the tellurium-containing molecules tend to move to the solution or to the surface of the coassemblies; thus, the signals of oxidized tellurium were observed. Utilizing Vc can reduce MTeC10-COONa to reduced states again; thus, MTeC10COONa molecules moved back to the interior of the coassemblies.

Characterization of the Product after Oxidation. Owing to the ultrasensitive ROS responsiveness of telluride-containing molecules, MTeC10COONa can be oxidized by a low concentration of H_2O_2. The oxidation product of the coassemblies was characterized by using ESI-MS negative spectra (Figure 5). After oxidation by 100 μM H_2O_2 for 1 h, the coassemblies can be easily oxidized to the oxidized state. As shown in Figure 5a, the ionic peak at 515.2 corresponding to MTeC10COONa with one oxygen atom added was found with typical isotopic peaks, and there were no peak for the reduced state of MTeC10COONa. An amplified scheme is shown in Figure 5b. When the oxidation time was extended to 5 h, the oxidized product remained a one-oxygen-atom-added structure, and typical isotopic peaks were also observed (Figure 5c,d). These results indicated that MTeC10COONa in coassemblies can be easily oxidized by 100 μM H_2O_2 to a structure with one oxygen atom added on tellurium. The morphology of oxidized 10:1 coassemblies was also studied by using TEM (Figure S8 in the SI). The results indicated that after oxidation the coassemblies were still spherical aggregates and tended to stack together.

Coassembly as a General Approach To Fabricate Reversible Redox Systems. The coassembly methodology can be employed as a general method to fabricate reversible redox systems. By using DPPE, another phospholipid to coassemble with MTeC10COONa, we can prepare a similar reversible redox system, of which the main driving force was hydrophobic interactions. Coassemblies of 10:1 (Figures 6 and S9 in the SI) and 4:1 (Figure S10 in the SI) were fabricated and characterized by DLS, TEM, SEM, EDS, and so on. As shown in Figure 6a, by using DLS, the average hydrodynamic diameter of the 10:1 coassemblies was confirmed to be 134 nm, and the average diameter measured by TEM was 34 nm (Figure 6b). EDS results (Figure 6c) also showed the existence of tellurium in the coassemblies, which showed the successful coassembly.

The reversible redox process of 10:1 coassemblies of DPPE and MTeC10COONa was also investigated by using ^{1}H NMR. As shown in Figure S11 in the SI, there was no peak of α or β protons of tellurium atoms of the original 10:1 coassemblies; after the addition of 2 equiv of H_2O_2, new broad peaks appeared at 2.85 and 1.87 ppm, which represented the α and β protons of tellurium atoms of the oxidized states, respectively. Also, upon reduction by 2 equiv of Vc, the broad peaks disappeared. This showed a phenomenon similar to that of the 10:1 coassemblies of DPPC and MTeC10COONa.

The product of 10:1 coassemblies of DPPE and MTeC10-COONa after oxidation and reduction was also characterized by a ESI-MS negative spectrum. In the presence of 100 μM H_2O_2 aqueous solution for 1 h, MTeC10COONa in the

DOI: 10.1021/acsami.5b04419
ACS Appl. Mater. Interfaces 2015, 7, 16054−16060

coassemblies can change to the oxidized state with one oxygen atom added, of which the molecular ionic peak is at 515.2 (m/z, $[M - H]^-$), with typical isotopic peaks, as shown in Figure S12a in the SI. The zoom-in scheme is shown in Figure S12b in the SI. When the oxidation time was increased to 5 h, the oxidized product remained a one-oxygen-atom-added structure, as shown in Figure S12c in the SI, and typical isotopic peaks were also observed (Figure S12d in the SI).

CONCLUSION AND OUTLOOK

In this work, we have successfully prepared a reversible redox system that was responsive to ultradiluted H_2O_2 (100 μM) by coassembling two different kinds of molecules: tellurium-containing molecules MTeC10COONa and phospholipid DPPC. The assembly behaviors and redox responsiveness were determined by DLS, TEM, SEM, ^{1}H NMR, and so on. This indicated that the MTeC10COONa molecules can be oxidized and reduced by 2 equiv of H_2O_2 and Vc, respectively. Also, in the presence of 100 μM H_2O_2, the MTeC10COONa molecules can be oxidized in 1 h. We also showed that the coassembly between MTeC10COONa and another phospholipid, DPPE can be realized. Thus, the coassembly between phophoslipid and tellurium-containing molecules can be empolyed as a general method to fabricate ultrasensitive ROS-responsive systems. Our preliminary study also showed that, by the coassembly of MTeC10COONa and DPPC, ion channels can be formed and switched on and off by redox stimuli (Figure S13 in the SI). Further experiments are currently ongoing.

ASSOCIATED CONTENT

Supporting Information

^{1}H and ^{13}C NMR and ESI-MS of MTeC10COOH, self-assembly properties of DPPC and MTeC10COONa, DLS, TEM, and SEM images of 4:1 and 1:1 coassemblies, and results of control experiments. The Supporting Information is available free of charge on the ACS Publications website at DOI: 10.1021/acsami.5b04419.

AUTHOR INFORMATION

Corresponding Author

*E-mail: xuhuaping@mail.tsinghua.edu.cn.

Notes

The authors declare no competing financial interest.

ACKNOWLEDGMENTS

This work was financially supported by the National Science Foundation for Distinguished Young Scholars (Grant 21425416), the National Basic Research Program of China (Grant 2013CB834502), the Foundation for Innovative Research Groups of the National Natural Science Foundation of China (Grant 21421064), and the National Natural Science Foundation of China (Grant 91427301).

REFERENCES

(1) Koide, Y.; Urano, Y.; Kenmoku, S.; Kojima, H.; Nagano, T. Design and Synthesis of Fluorescent Probes for Selective Detection of Highly Reactive Oxygen Species in Mitochondria of Living Cells. *J. Am. Chem. Soc.* **2007**, *129*, 10324−10325.

(2) Valentine, J. S.; Gralla, E. B. Reactive Oxygen Species Special Feature. *Proc. Natl. Acad. Sci. U. S. A.* **2008**, *105*, 8178.

(3) Joshi-Barr, S.; de Gracia Lux, C.; Mahmoud, E.; Almutairi, A. Exploiting Oxidative Microenvironments in the Body as Triggers for Drug Delivery Systems. *Antioxid. Redox Signaling* **2014**, *21*, 730−754.

(4) Phillips, D. J.; Gibson, M. I. Redox-Sensitive Materials for Drug Delivery: Targeting the Correct Intracellular Environment, Tuning Release Rates, and Appropriate Predictive Systems. *Antioxid. Redox Signaling* **2014**, *21*, 786−803.

(5) Finkel, T. Signal Transduction by Reactive Oxygen Species. *J. Cell Biol.* **2011**, *194*, 7−15.

(6) Forman, H. J.; Torres, M. Reactive Oxygen Species and Cell Signaling: Respiratory Burst in Macrophage Signaling. *Am. J. Respir. Crit. Care Med.* **2002**, *166*, S4−S8.

(7) Ray, P. D.; Huang, B. W.; Tsuji, Y. Reactive Oxygen Species (ROS) Homeostasis and Redox Regulation in Cellular Signaling. *Cell. Signalling* **2012**, *24*, 981−990.

(8) Thannickal, V. J.; Fanburg, B. L. Reactive Oxygen Species in Cell Signaling. *Am. J. Physiol. Lung Cell. Mol. Physiol.* **2000**, *279*, L1005−L1028.

(9) Alfadda, A. A.; Sallam, R. M. Reactive Oxygen Species in Health and Disease. *J. Biomed. Biotechnol.* **2012**, 936486.

(10) Brieger, K.; Schiavone, S.; Miller, F. J., Jr.; Krause, K. H. Reactive Oxygen Species: From Health to Disease. *Swiss Med. Wkly.* **2012**, *142*, w13659.

(11) Yang, G.; Yuan, H.; Zhu, C.; Liu, L.; Yang, Q.; Lv, F.; Wang, S. New Conjugated Polymers for Photoinduced Unwinding of DNA Supercoiling and Gene Regulation. *ACS Appl. Mater. Interfaces* **2012**, *4*, 2334−2337.

(12) Harman, D. The Aging Process. *Proc. Natl. Acad. Sci. U. S. A.* **1981**, *78*, 7124−7128.

(13) Krause, K. H. Aging: A Revisited Theory Based on Free Radicals Generated by Nox Family Nadph Oxidases. *Exp. Gerontol.* **2007**, *42*, 256−262.

(14) Zhang, Y.; Dawson, V. L.; Dawson, T. M. Oxidative Stress and Genetics in the Pathogenesis of Parkinson's Disease. *Neurobiol. Dis.* **2000**, *7*, 240−250.

(15) Block, M. L. NADPH Oxidase as a Therapeutic Target in Alzheimer's Disease. *BMC Neurosci.* **2008**, *9* (Suppl 2), S8.

(16) Sugamura, K.; Keaney, J. F., Jr. Reactive Oxygen Species in Cardiovascular Disease. *Free Radical Biol. Med.* **2011**, *51*, 978.

(17) Schumacker, P. T. Reactive Oxygen Species in Cancer: A Dance with the Devil. *Cancer Cell* **2015**, *27*, 156−157.

(18) Costa, A.; Scholer-Dahirel, A.; Mechta-Grigoriou, F. The Role of Reactive Oxygen Species and Metabolism on Cancer Cells and Their Microenvironment. *Semin. Cancer Biol.* **2014**, *25*, 23−32.

(19) Shiao, Y. S.; Chiu, H. H.; Wu, P. H.; Huang, Y. F. Aptamer-Functionalized Gold Nanoparticles as Photoresponsive Nanoplatform for Co-Drug Delivery. *ACS Appl. Mater. Interfaces* **2014**, *6*, 21832−21841.

(20) Stegemann, L.; Schuermann, K. C.; Strassert, C. A.; Grecco, H. E. Photofunctional Surfaces for Quantitative Fluorescence Microscopy: Monitoring the Effects of Photogenerated Reactive Oxygen Species at Single Cell Level with Spatiotemporal Resolution. *ACS Appl. Mater. Interfaces* **2015**, *7*, 5944−5949.

(21) An, Q.; Sun, C.; Li, D.; Xu, K.; Guo, J.; Wang, C. Peroxidase-Like Activity of Fe_3o_4@Carbon Nanoparticles Enhances Ascorbic Acid-Induced Oxidative Stress and Selective Damage to Pc-3 Prostate Cancer Cells. *ACS Appl. Mater. Interfaces* **2013**, *5*, 13248−13257.

(22) Bedard, K.; Krause, K.-H. The Nox Family of ROS-Generating Nadph Oxidases: Physiology and Pathophysiology. *Physiol. Rev.* **2007**, *87*, 245−313.

(23) Cifuentes-Pagano, E.; Meijles, D. N.; Pagano, P. J. The Quest for Selective Nox Inhibitors and Therapeutics: Challenges, Triumphs and Pitfalls. *Antioxid. Redox Signaling* **2014**, *20*, 2741−2754.

(24) Muhammad, F.; Wang, A.; Qi, W.; Zhang, S.; Zhu, G. Intracellular Antioxidants Dissolve Man-Made Antioxidant Nanoparticles: Using Redox Vulnerability of Nanoceria to Develop a Responsive Drug Delivery System. *ACS Appl. Mater. Interfaces* **2014**, *6*, 19424−19433.

DOI: 10.1021/acsami.5b04419
ACS Appl. Mater. Interfaces 2015, 7, 16054−16060

(25) Cao, W.; Zhang, X.; Miao, X.; Yang, Z.; Xu, H. Gamma-Ray-Responsive Supramolecular Hydrogel Based on a Diselenide-Containing Polymer and a Peptide. *Angew. Chem., Int. Ed.* **2013**, *52*, 6233−6237.
(26) Ma, N.; Li, Y.; Xu, H.; Wang, Z.; Zhang, X. Dual Redox Responsive Assemblies Formed from Diselenide Block Copolymers. *J. Am. Chem. Soc.* **2010**, *132*, 442−443.
(27) Ma, N.; Xu, H.; An, L.; Li, J.; Sun, Z.; Zhang, X. Radiation-Sensitive Diselenide Dlock Co-Polymer Micellar Aggregates: Toward the Combination of Radiotherapy and Chemotherapy. *Langmuir* **2011**, *27*, 5874−5878.
(28) Han, P.; Ma, N.; Ren, H.; Xu, H.; Li, Z.; Wang, Z.; Zhang, X. Oxidation-Responsive Micelles Based on a Selenium-Containing Polymeric Superamphiphile. *Langmuir* **2010**, *26*, 14414−14418.
(29) Ma, N.; Li, Y.; Ren, H.; Xu, H.; Li, Z.; Zhang, X. Selenium-Containing Block Copolymers and Their Oxidation-Responsive Aggregates. *Polym. Chem.* **2010**, *1*, 1609−1614.
(30) Xu, H.; Cao, W.; Zhang, X. Selenium-Containing Polymers: Promising Biomaterials for Controlled Release and Enzyme Mimics. *Acc. Chem. Res.* **2013**, *46*, 1647−1658.
(31) Cao, W.; Gu, Y.; Meineck, M.; Xu, H. The Combination of Chemotherapy and Radiotherapy Towards More Efficient Drug Delivery. *Chem. - Asian J.* **2014**, *9*, 48−57.
(32) Wang, L.; Cao, W.; Yi, Y.; Xu, H. Dual Redox Responsive Coassemblies of Diselenide-Containing Block Copolymers and Polymer Lipids. *Langmuir* **2014**, *30*, 5628−5636.
(33) Ji, S.; Cao, W.; Xu, H. A ROS Eliminating Nanocomposite Film Fabricated from Diselenide-Containing Polymer Micelles. *Part. Part. Syst. Charact.* **2013**, *30*, 1034−1038.
(34) Ramadan, S. E.; Razak, A. A.; Ragab, A. M.; El-Meleigy, M. Incorporation of Tellurium into Amino Acids and Proteins in a Tellurium-Tolerant Fungi. *Biol. Trace Elem. Res.* **1989**, *20*, 225−232.
(35) Ren, X.; Xue, Y.; Liu, J.; Zhang, K.; Zheng, J.; Luo, G.; Guo, C.; Mu, Y.; Shen, J. A Novel Cyclodextrin-Derived Tellurium Compound with Glutathione Peroxidase Activity. *ChemBioChem* **2002**, *3*, 356−363.
(36) Dong, Z.; Liu, J.; Mao, S.; Huang, X.; Luo, G.; Shen, J. A Glutathione Peroxidase Mimic 6,6′-Ditellurobis (6-Deoxy-B-Cyclodextrin) with High Substrate Specificity. *J. Inclusion Phenom. Mol. Recognit. Chem.* **2006**, *56*, 179−182.
(37) Lin, T.; Ding, Z.; Li, N.; Xu, J.; Luo, G.; Liu, J.; Shen, J. 2-Tellurium-Bridged Beta-Cyclodextrin, a Thioredoxin Reductase Inhibitor, Sensitizes Human Breast Cancer Cells to Trail-Induced Apoptosis through Dr5 Induction and Nf-Kappab Suppression. *Carcinogenesis* **2011**, *32*, 154−167.
(38) Avila, D. S.; Benedetto, A.; Au, C.; Manarin, F.; Erikson, K.; Soares, F. A.; Rocha, J. B. T.; Aschner, M. Organotellurium and Organoselenium Compounds Attenuate Mn-Induced Toxicity in Caenorhabditis Elegans by Preventing Oxidative Stress. *Free Radical Biol. Med.* **2012**, *52*, 1903−1910.
(39) Mao, S.; Dong, Z.; Liu, J.; Li, X.; Liu, X.; Luo, G.; Shen, J. Semisynthetic Tellurosubtilisin with Glutathione Peroxidase Activity. *J. Am. Chem. Soc.* **2005**, *127*, 11588−11589.
(40) Cao, W.; Gu, Y.; Meineck, M.; Li, T.; Xu, H. Tellurium-Containing Polymer Micelles: Competitive-Ligand-Regulated Coordination Responsive Systems. *J. Am. Chem. Soc.* **2014**, *136*, 5132−5137.
(41) Cao, W.; Wang, L.; Xu, H. Coordination Responsive Tellurium-Containing Multilayer Film for Controlled Delivery. *Chem. Commun.* **2015**, *51*, 5520−5522.
(42) Wang, X.; Hu, J.; Zhang, G.; Liu, S. Highly Selective Fluorogenic Multianalyte Biosensors Constructed Via Enzyme-Catalyzed Coupling and Aggregation-Induced Emission. *J. Am. Chem. Soc.* **2014**, *136*, 9890−9893.
(43) de Gracia Lux, C.; Joshi-Barr, S.; Nguyen, T.; Mahmoud, E.; Schopf, E.; Fomina, N.; Almutairi, A. Biocompatible Polymeric Nanoparticles Degrade and Release Cargo in Response to Biologically Relevant Levels of Hydrogen Peroxide. *J. Am. Chem. Soc.* **2012**, *134*, 15758−15764.
(44) Stuart, M. A. C.; Huck, W. T. S.; Genzer, J.; Muller, M.; Ober, C.; Stamm, M.; Sukhorukov, G. B.; Szleifer, I.; Tsukruk, V. V.; Urban, M.; Winnik, F.; Zauscher, S.; Luzinov, I.; Minko, S. Emerging Applications of Stimuli-Responsive Polymer Materials. *Nat. Mater.* **2010**, *9*, 101−113.
(45) Cao, W.; Gu, Y.; Li, T.; Xu, H. Ultra-Sensitive ROS-Responsive Tellurium-Containing Polymers. *Chem. Commun.* **2015**, *51*, 7069−7071.
(46) Kraft, J. C.; Freeling, J. P.; Wang, Z.; Ho, R. J. Y. Emerging Research and Clinical Development Trends of Liposome and Lipid Nanoparticle Drug Delivery Systems. *J. Pharm. Sci.* **2014**, *103*, 29−52.
(47) Torchilin, V. P. Recent Advances with Liposomes as Pharmaceutical Carriers. *Nat. Rev. Drug Discovery* **2005**, *4*, 145−160.
(48) Chandrawati, R.; Caruso, F. Biomimetic Liposome- and Polymersome-Based Multicompartmentalized Assemblies. *Langmuir* **2012**, *28*, 13798−13807.
(49) Paleos, C. M.; Tsiourvas, D.; Sideratou, Z. Preparation of Multicompartment Lipid-Based Systems Based on Vesicle Interactions. *Langmuir* **2012**, *28*, 2337−2346.
(50) Behanna, H. A.; Donners, J. J. J. M.; Gordon, A. C.; Stupp, S. I. Coassembly of Amphiphiles with Opposite Peptide Polarities into Nanofibers. *J. Am. Chem. Soc.* **2005**, *127*, 1193−1120.
(51) Groschel, A. H.; Walther, A.; Lobling, T. I.; Schacher, F. H.; Schmalz, H.; Muller, A. H. Guided Hierarchical Co-Assembly of Soft Patchy Nanoparticles. *Nature* **2013**, *503*, 247−251.
(52) Han, Y.; Wang, W.; Tang, Y.; Zhang, S.; Li, Z.; Wang, Y. Coassembly of Poly(Ethylene Glycol)-Block-Poly(Glutamate Sodium) and Gemini Surfactants with Different Spacer Lengths. *Langmuir* **2013**, *29*, 9316−9323.
(53) Therien-Aubin, H.; Lukach, A.; Pitch, N.; Kumacheva, E. Coassembly of Nanorods and Nanospheres in Suspensions and in Stratified Films. *Angew. Chem., Int. Ed.* **2015**, *54*, 5618−5622.
(54) Fan, W.; Zhang, C.; Tjiu, W. W.; Pramoda, K. P.; He, C.; Liu, T. Graphene-Wrapped Polyaniline Hollow Spheres as Novel Hybrid Electrode Materials for Supercapacitor Applications. *ACS Appl. Mater. Interfaces* **2013**, *5*, 3382−3391.
(55) Bairi, P.; Roy, B.; Chakraborty, P.; Nandi, A. K. Co-Assembled White-Light-Emitting Hydrogel of Melamine. *ACS Appl. Mater. Interfaces* **2013**, *5*, 5478−5485.
(56) Islam, M. S.; Choi, W. S.; Lee, H. J. Controlled Etching of Internal and External Structures of Sio2 Nanoparticles Using Hydrogen Bond of Polyelectrolytes. *ACS Appl. Mater. Interfaces* **2014**, *6*, 9563−9571.
(57) Spink, C. H.; Lieto, V.; Mereand, E.; Pruden, C. Micelle-Vesicle Transition in Phospholipid-Bile Salt Mixtures. A Study by Precision Scanning Calorimetry. *Biochemistry* **1991**, *30*, 5104−5112.
(58) De la Maza, A.; Parra, J. L. Vesicle-Micelle Structural Transition of Phosphatidylcholine Bilayers and Triton X-100. *Biochem. J.* **1994**, *303*, 907−914.
(59) Andelman, D.; Kozlov, M. M.; Helfrich, W. Phase Transitions between Vesicles and Micelles Driven by Competing Curvatures. *Europhys. Lett.* **1994**, *25*, 231−236.
(60) Stuart, M. C.; Boekema, E. J. Two Distinct Mechanisms of Vesicle-to-Micelle and Micelle-to-Vesicle Transition Are Mediated by the Packing Parameter of Phospholipid-Detergent Systems. *Biochim. Biophys. Acta, Biomembr.* **2007**, *1768*, 2681−2689.
(61) Elsayed, M. M.; Cevc, G. The Vesicle-to-Micelle Transformation of Phospholipid-Cholate Mixed Aggregates: A State of the Art Analysis Including Membrane Curvature Effects. *Biochim. Biophys. Acta, Biomembr.* **2011**, *1808*, 140−153.

DOI: 10.1021/acsami.5b04419
ACS Appl. Mater. Interfaces 2015, 7, 16054−16060